Available online at www.sciencedirect.com
SCIENCE DIRECT®
Sensors and Actuators A 104 (2003) 132–142
SENSORS AND ACTUATORS A PHYSICAL
www.elsevier.com/locate/sna

Design and control of a thermal stabilizing system for a MEMS optomechanical uncooled infrared imaging camera

Jongeun Choi, Joji Yamaguchi, Simon Morales, Roberto Horowitz*, Yang Zhao, Arunava Majumdar

Department of Mechanical Engineering, University of California at Berkeley, 6193 Etcheverry Hall, Berkeley, CA 94720-1742, USA

Abstract

In this paper, the design and control of a thermal stabilizing system for an optomechanical uncooled infrared (IR) imaging camera is presented, which uses an array of MEMS bimaterial cantilever beams to sense an IR image source. A one-dimensional lumped parameter model of the thermal stabilization system was derived and experimentally validated. A model-based discrete time linear quadratic gaussian regulator (LQGR) control scheme, with a stochastic ambient noise model, was implemented. The control system incorporates a reference model, which generates desired reference temperature trajectory, and integral action to respectively diminish overshoots and achieve zero steady state error in closed loop. Simulation results show that the designed LQGR is able to enhance ambient temperature low frequency disturbance attenuation by more than 50 dB. The control system is able to regulate the focal-plane array (FPA) temperature with a standard deviation of about 100 μK, in spite of the fact that the temperature measurement noise has a standard deviation of 1 mK. Noise analysis results for the present stage of the optomechanical IR imaging system are summarized. The noise equivalent temperature difference (NETD) of the current stage of the IR camera system can achieve about 200 mK.

Keywords: MEMS IR sensors; Infrared image detectors; Temperature control; LQGR control; Stochastic modeling; NETD

1. Introduction

In many engineering applications involving temperature sensitivity issues, it is required that the temperature be regulated to within some operating range. Temperature stabilization systems have been discussed in many publications. Temperature regulators that utilize Peltier junction heat pumps and conventional PID controllers are commonly used nowadays [1]. The temperature control system design presented in this paper is part of a novel optomechanical uncooled infrared imaging system, which utilizes an array of MEMS bimaterial cantilever beams, and it is currently under development by the authors of this paper [2,3]. Infrared (IR) vision is an indispensable technology for night vision, surveillance and navigation through obscure environments. Our uncooled IR imaging system consists of an absorption pad for IR radiation and a focal-plane array (FPA) of about 300 pixels × 300 pixels (pixel size of 65 μm × 65 μm), with each pixel containing a bimaterial cantilever beam built based on the MEMS technology, and shown in Fig. 1, or as in [2]. Fig. 2 shows the overall view of the our micro-optomechanical uncooled infrared receiver with optical readout system. Each pixel in the FPA array consists of a bimaterial cantilever beam, which bends as its temperature rises due to absorption of the incident infrared radiation. The cantilever deflection is proportional to the change in temperature of the beam and also to the difference between the thermal expansion coefficients of the two cantilever materials. An optical system using visible light simultaneously measures the deflections of all the cantilevers of the FPA by interferometry, and projects a visible image onto a visible charge-coupled device (CCD) as shown in Fig. 2. A first prototype of such an infrared system, which did not utilize a thermal control system such as the one presented in this paper, was described in [4]. The new design has MEMS cantilevers that have a much larger sensitivity than those in the design presented in [4], requires that the FPA temperature be regulated to within a standard deviation of 100 μK to be close to the CCD shot noise level of 65 μK, which is another dominant noise level of the system. This paper describes the design of a thermal stabilizing system for the IR imaging system. The design was carried out in

* Corresponding author. Tel.: +1-510-642-4675; fax: +1-510-642-6163.
E-mail address: horowitz@me.berkeley.edu (R. Horowitz).

0924-4247/03/$ – see front matter © 2003 Elsevier Science B.V. All rights reserved.
doi:10.1016/S0924-4247(03)00004-9

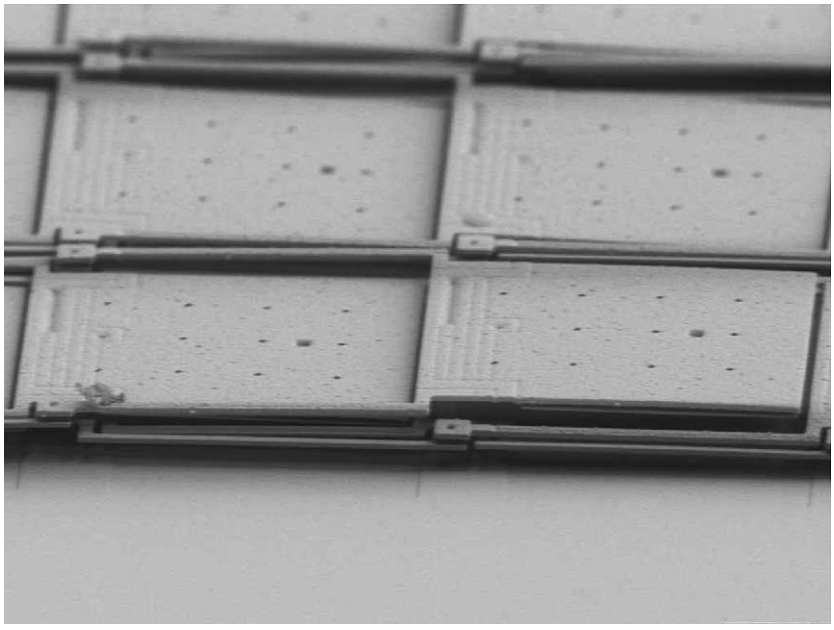

Fig. 1. FPA built on MEMS technology.

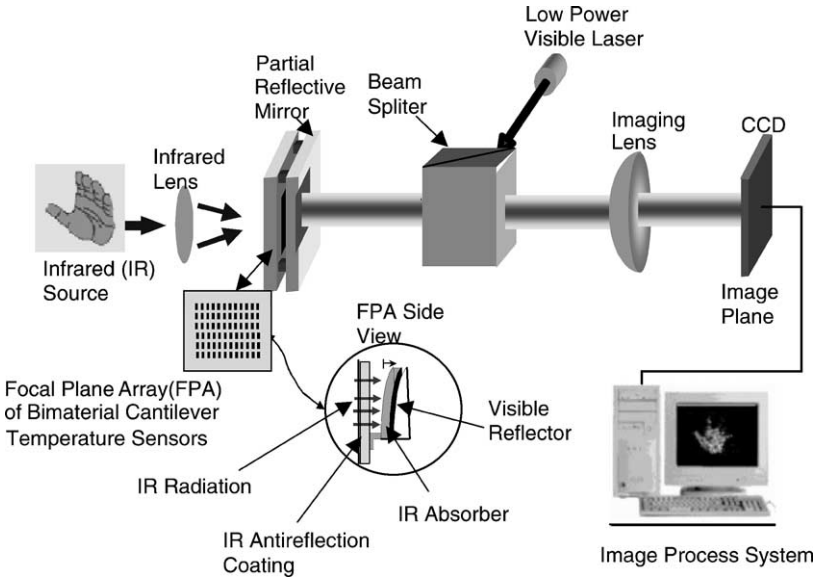

Fig. 2. Optomechanical uncooled infrared imaging camera system.

two stages. In the first stage a passive thermal shield design was invented to maximize the attenuation of ambient temperature fluctuations while still maintaining a high sensitivity to the IR source. The second stage of the design involved feedback control. After obtaining stochastic models of the ambient temperature noise disturbances and sensor noise, a Kalman filter observer was designed to estimate the FPA temperature and a linear quadratic gaussian regulator was implemented to regulate the FPA temperature. The control system was designed in order to enhance low frequency ambient temperature disturbance attenuation without significantly degrading the device's sensitivity to the target IR temperature. Part of this paper without the theoretical and experimental system noise analysis, was presented in the 15th IFAC World Congress [5].

2. Design and modeling

A SEM photograph of the fabricated FPA is shown in Fig. 1. A schematic depiction of the camera is shown in Fig. 3. The bimaterial cantilever deflection, as its temperature rises due to absorption of the incident infrared radiation, is proportional to the change in temperature of the beam and

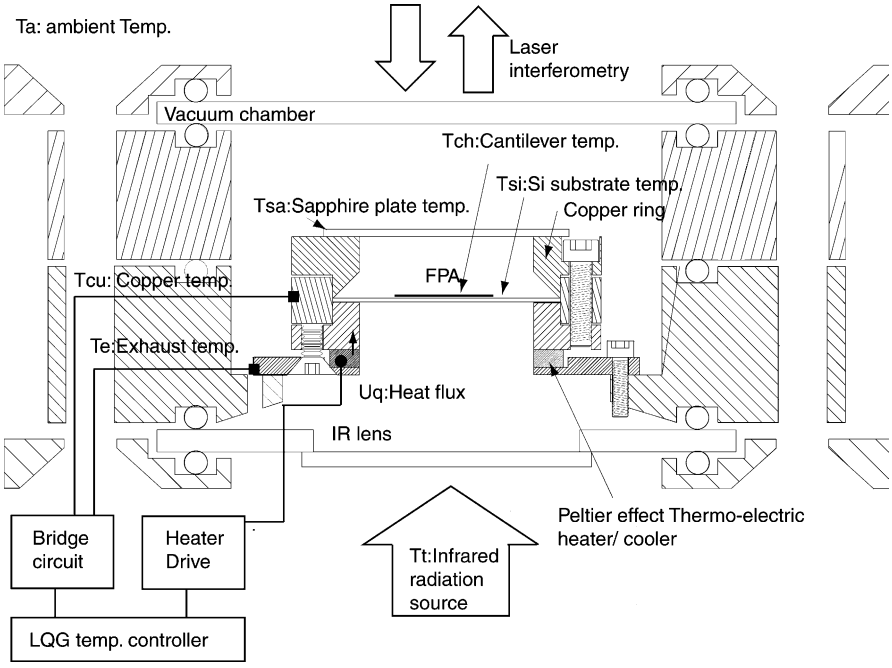

Fig. 3. A schematic setup of the IR camera and its temperature control system. The CCD and optical readout system is outside of the vacuum chamber.

also to the difference between the thermal expansion coefficients of the two cantilever materials. An optical system using visible light simultaneously measures the deflections of all the cantilevers of the FPA, and collectively projects a visible image of the spatially-varying IR radiation onto a visible CCD or CMOS array. As shown in Fig. 3, the FPA is surrounded by a heat shield, which consists of a copper cylinder and a thermally conductive sapphire plate. This shield isolates the FPA from fluctuations in the ambient temperature T_a. The sapphire plate is transparent to laser light, allowing the laser to be used as an interferometry measurement system to obtain an image from the FPA. A

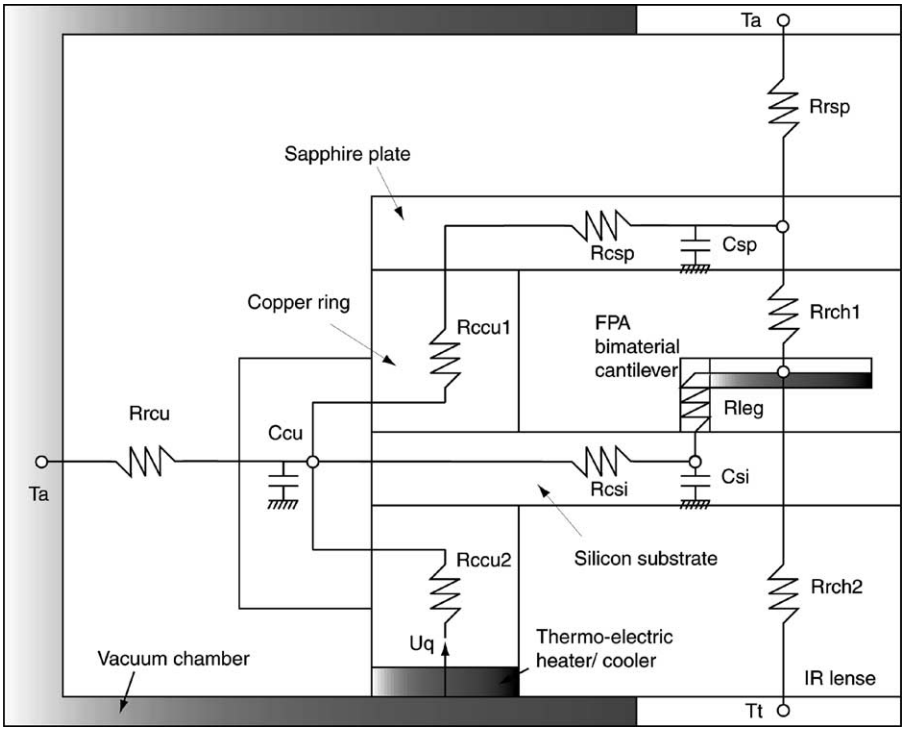

Fig. 4. A schematic diagram of lumped parameter modeling.

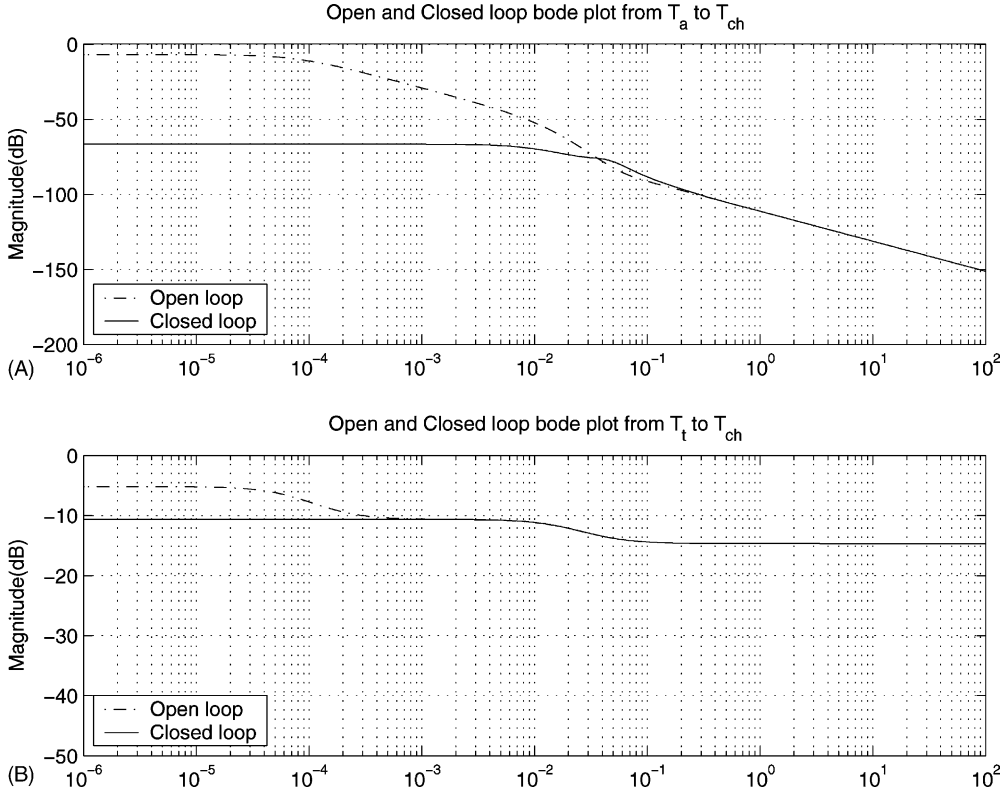

Fig. 5. Open-loop and closed-loop Bode plot for (A) T_a to T_{ch} and (B) T_t to T_{ch}. The systems are non-minimum phase.

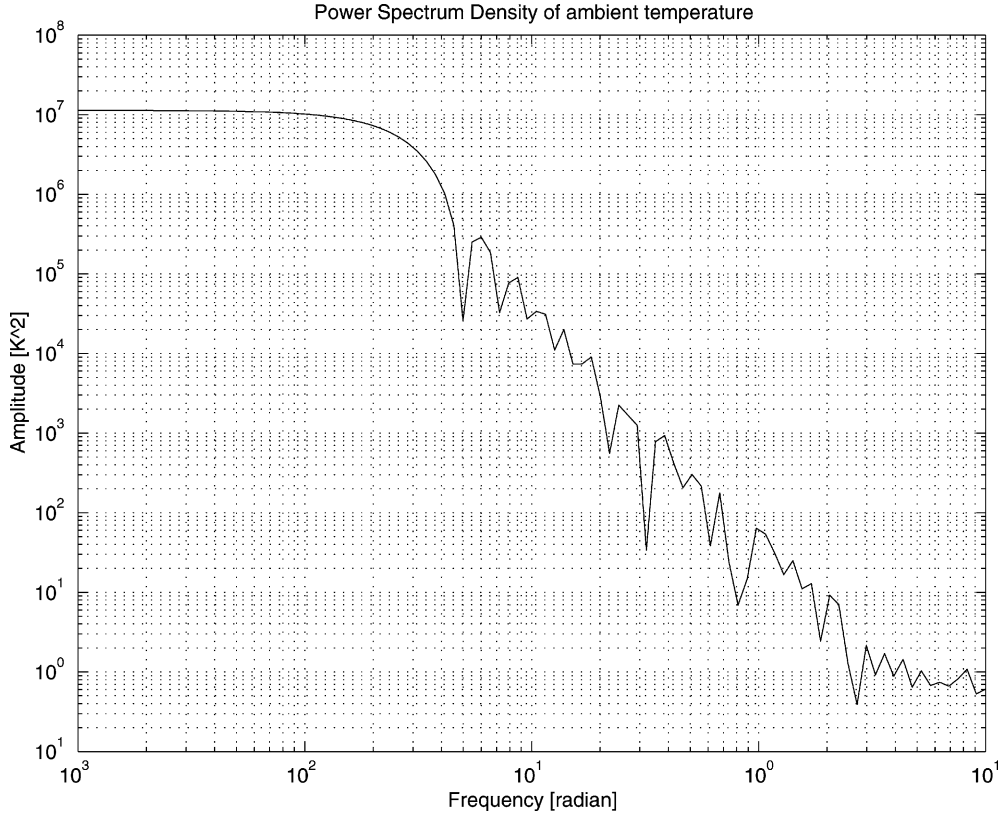

Fig. 6. Power spectrum density of ambient temperature.

thermo-electric Peltier junction heater/cooler [11] comprises the thermal actuator, which is capable of adding heat to or removing heat from the system. A thermistor on the side of the copper ring senses its temperature T_{cu}. Another thermistor is attached to the vacuum chamber to measure the deterministic initial ambient temperature. The thermal shield has a low thermal resistance for the copper cylinder (R_{ccu1}), as shown Fig. 4 and so does the sapphire plate. However the thermal resistance between the FPA and the copper cylinder (R_{csi}) is chosen to be relatively high, in order to isolate the FPA from the regulated thermal shield. As a consequence, the thermal system provides a large amount of attenuation in open loop (-50 to -100 dB) in the range of (0.002–10 Hz) from the disturbance T_a to FPA temperature T_{ch}, as shown in Fig. 5. An one-dimensional lumped parameter model [9] was used to model the thermal system, taking into account of thermal capacitance and thermal resistance of the copper block and sapphire and silicon plates in Fig. 4.

Fig. 6 shows the power spectrum density of the measured ambient temperature in the lab where the IR imaging system is located. Based on this data, a model for the ambient temperature fluctuations was derived which consists of a critically damped second-order linear dynamic system with a cut-off frequency of 2.5×10^{-2} rad, which is excited by zero mean white noise $w(t)$ $E(w(i)w(j)^{\mathrm{T}}) = W\delta_{ij}$, where $W = 1600\,\mathrm{K}^2$ (obtained from the measurement in Fig. 6) and δ_{ij} is the Kronecker delta. A high-sensitivity thermistor and analog bridge circuit were used to measure the copper ring temperature with a 1 mK measurement noise standard deviation.

3. Control law

3.1. The Kalman filter for the linearized plant

The closed-loop system was designed based on a discrete-time linearized thermal plant that included the third-order lumped parameter thermal model depicted in Fig. 4, the identified ambient temperature stochastic noise model and an empirically found thermal actuator dynamic model. The linearized thermal plant is obtained as follows

$$\begin{aligned} x_p(t+1) &= A_p x_p(t) + B_p U_p(t) \\ y_p(t) &= C_p x_p(t) + D_p U_p(t) \end{aligned} \tag{1}$$

where

$$A_p = \begin{bmatrix} 9.998 \times 10^{-1} & 1.438 \times 10^{-4} & 2.348 \times 10^{-5} \\ 1.022 \times 10^{-3} & 9.989 \times 10^{-1} & 1.101 \times 10^{-6} \\ 1.776 \times 10^{-3} & 1.173 \times 10^{-5} & 9.979 \times 10^{-1} \end{bmatrix}$$

$$B_p = \begin{bmatrix} 2.297 \times 10^{-3} & 7.832 \times 10^{-7} & 3.337 \times 10^{-9} \\ 1.174 \times 10^{-6} & 3.610 \times 10^{-5} & 2.497 \times 10^{-7} \\ 2.041 \times 10^{-6} & 9.050 \times 10^{-10} & 2.824 \times 10^{-4} \end{bmatrix}$$

$$C_p = \begin{bmatrix} 1.00 & 0 & 0 \\ 0 & 0 & 1.00 \\ 0 & 7.5976 \times 10^{-3} & 8.0761 \times 10^{-1} \end{bmatrix}$$

$$D_p = \begin{bmatrix} 0 & 0 & 0 \\ 0 & 0 & 0 \\ 0 & 0 & 1.8479 \times 10^{-1} \end{bmatrix}$$

The state of the thermal plant is $x_p = [T_{cu} \quad T_{sa} \quad T_{si}]^{\mathrm{T}}$, where T_{cu} is the copper ring temperature, T_{sa} is the sapphire plate temperature and T_{si} is the silicon substrate temperature. Control input to the plant is $U_p = [u_q \quad T_a \quad T_t]^{\mathrm{T}}$, where u_q (J/s or W) is control input or heat flux from the heater/cooler, T_a is the ambient temperature, and T_t is the target temperature. The empirically found first-order linear low-pass filter type actuator dynamic is give by

$$\begin{aligned} x_f(t+1) &= 0.9802 x_f(t) + 0.2500 u_q(t) \\ y_{\mathrm{actuator}}(t) &= 0.15841 x_f(t) \end{aligned} \tag{2}$$

An augmented system for the observer and the controller was constructed, as shown in Fig. 7.

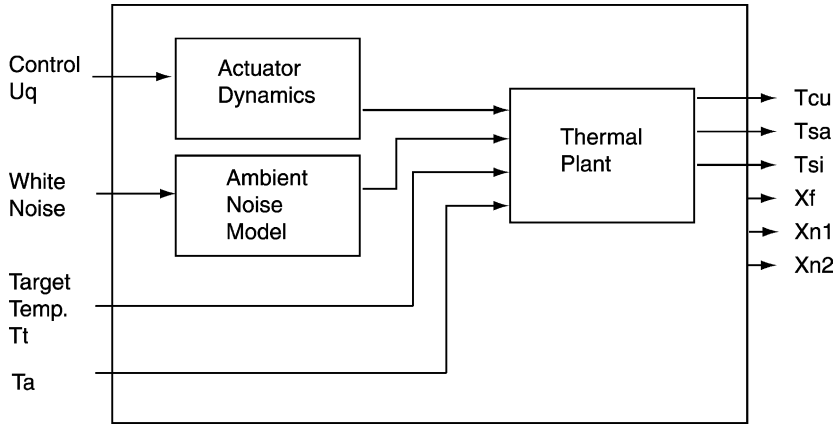

Fig. 7. Augmented system with a linearized thermal plant, an actuator model and an stochastic noise model.

The augmented system consists of the plant state x_p, the actuator state x_f, and the noise model state $x_N = [x_{n1} \quad x_{n2}]^T$. The state x_N is not controllable from the control input $u_q(t)$ but is stable and it is only of a stochastic nature.

$$\begin{pmatrix} x_p(t+1) \\ x_f(t+1) \\ x_N(t+1) \end{pmatrix} = A_a \begin{pmatrix} x_p(t) \\ x_f(t) \\ x_N(t) \end{pmatrix} + B_a \begin{pmatrix} u_q \\ T_a \\ T_t \end{pmatrix} + G_a w(t)$$

i.e.

$$\begin{aligned} X_a(t+1) &= A_{a(6\times6)} X_a(t) + B_{a(6\times3)} u_a(t) + G_a w(t) \\ y_a(t) &= C_a X_a(t) + v(t) \end{aligned} \tag{3}$$

where $w(t)$ and $v(t)$ are white noises, which have the following properties

$$E(w(t)) = 0, \quad E(w(i)w(j)^T) = W\delta_{ij}$$
$$E(v(t)) = 0, \quad E(v(i)v(j)^T) = V\delta_{ij}$$

In addition, the deterministic mean values of the ambient and target temperatures, respectively T_a and T_t, are also considered as inputs to the system given by Eq. (3)and depicted in Fig. 7. The output of this system is the copper cylinder temperature T_{cu}, only which is penalized by the controller. Therefore, the corresponding B_a and C_a are

$$B_a = [B_{a1(6\times1)} \quad B_{a2(6\times1)} \quad B_{a3(6\times1)}]$$

$$C_a = [1 \quad 0 \quad 0 \quad 0 \quad 0 \quad 0]$$

Given the detectable pair (A_a, C_a) and the stabilizable (A_a, B_a), there exists a steady state Kalman filter gain, which is given by $M_s = \Sigma_s C^T (C\Sigma_s C^T + V)^{-1}$, where Σ_s is the solution of the following algebraic Riccati equation

$$\Sigma_s = A_a \Sigma_s A_a^T + G_a W G_a^T - A_a \Sigma_s C^T (C\Sigma_s C^T + V)^{-1} C\Sigma_s A_a^T \tag{4}$$

Using the Kalman filter gain M_s from Eq. (4) and the system parameters in Eq. (3), an optimal state estimator can be constructed as follows

$$\begin{aligned} \hat{X}_a(t+1|t+1) = (I - M_s C_a) A_a \hat{X}_a(t|t) + (I - M_s C_a) B_a u(t) \\ + M_s y(t+1) \end{aligned} \tag{5}$$

3.2. Integral action and reference model for the desired trajectory

An integral action control was implemented to compensate for the detrimental effects of constant disturbances [6,8]. Define the tracking error as $e(t) = y_a(t) - y_r$, where $y_a = T_{cu}$ is the copper ring temperature and $y_r = T_{cur}$ is the reference temperature trajectory. The incremental tracking error integral is given by

$$I(t+1) = I(t) + e(t) = I(t) + C_a X_a(t) - y_r \tag{6}$$

A second-order linear dynamic system with a unit static gain was chosen for the reference model. The response time of the system was fixed to about 200 s, but it can be controlled by modifying this reference model dynamic.

$$\begin{aligned} x_r(t+1) &= A_{r(2\times2)} x_r(t) + B_{r(2\times1)} u_r(t) \\ y_r(t) &= C_{r(1\times2)} x_r(t) \end{aligned} \tag{7}$$

Utilizing Eqs. (7) and (6) with the plant model Eq. (3) the linear quadratic tracking problem can be reformulated into a standard linear quadratic regulation of the following composite system with an extended state.

$$x^{track}(t) = \begin{pmatrix} X_a(t) \\ I(t) \\ x_r(t) \end{pmatrix}$$

The state equation for $x^{track}(t)$ is then obtained by combining the state equations of $X_a(t)$, $I(t)$ and $x_r(t)$; $u_r(t)$ is a constant set-point.

$$\begin{aligned} x^{track}(t+1) = &\begin{bmatrix} A_{a(6\times6)} & 0_{6\times1} & 0_{6\times2} \\ C_a & 1 & -C_{r(1\times2)} \\ 0_{2\times6} & 0_{2\times1} & A_{r(2\times2)} \end{bmatrix} x^{track}(t) \\ &+ \begin{bmatrix} B_{a1(6\times1)} & 0_{7\times1} \\ 0_{3\times1} & B_{r(2\times1)} \end{bmatrix} \begin{pmatrix} u_q(t) \\ u_r(t) \end{pmatrix} \end{aligned} \tag{8}$$

y_t^{track} is given by

$$\begin{aligned} y^{track}(t) &= (y_a(t) - y_r(t)) + g_e I(t) \\ y^{track}(t) &= C^{track} x^{track}(t) = [C_a \quad g_e \quad -Cr] x^{track}(t) \end{aligned} \tag{9}$$

where g_e is the weighting factor between the tracking error and the incremental tracking error. The backward-shift operator or delay operator is denoted by q^{-1} such that $q^{-1}g(t) = g(t-1)$. By multiplying each side of Eq. (8) by the difference operator $(1 - q^{-1})$ and considering $u_r(t)$ to be a constant desired set-point, we can obtain

$$\begin{aligned} (1-q^{-1}) x^{track}(t+1) &= \begin{pmatrix} (1-q^{-1}) X_a(t+1) \\ (1-q^{-1}) I(t+1) \\ (1-q^{-1}) x_r(t+1) \end{pmatrix} \\ &= \begin{pmatrix} x_d(t) \\ e(t) \\ x_{rd}(t) \end{pmatrix} = x_d^{track}(t) \end{aligned}$$

likewise,

$$(1-q^{-1}) A^{track} x(t)^{track} = A^{track} x_d^{track}(t)$$

However, the constant input $u_r(t)$ is gone after taking the difference operator, since $u_r(t) = u_r(t+1)$.

$$(1-q^{-1}) \begin{bmatrix} 0_{7\times1} \\ B_{r(2\times1)} \end{bmatrix} u_r(t) = 0$$

Define $v(t-1)$ such as $v(t-1) = (1-q^{-1})u_q(t)$. Multiplying difference operator to Eq. (8) leads to

$$\begin{aligned} \begin{pmatrix} x_d(t) \\ e(t) \\ x_r d(t) \end{pmatrix} = &A^{track} \begin{pmatrix} x_d(t-1) \\ e(t-1) \\ x_r d(t-1) \end{pmatrix} \\ &+ \begin{bmatrix} B_{a1(6\times1)} \\ 0_{3\times1} \end{bmatrix} ((1-q^{-1}) u_q(t) = v(t-1)) \end{aligned}$$

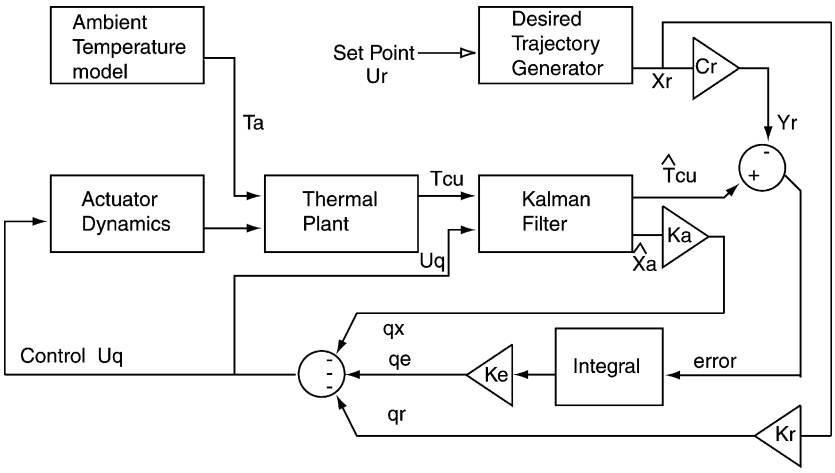

Fig. 8. LQGR with desired trajectory control scheme.

i.e.

$$x_{\mathrm{d}}^{\mathrm{track}}(t) = A^{\mathrm{track}}x_{\mathrm{d}}^{\mathrm{track}}(t-1) + B^{\mathrm{track}}v(t-1)$$
$$y_{\mathrm{d}}^{\mathrm{track}}(t-1) = C_{\mathrm{a}}x_{\mathrm{d}}(t-1) - C_{\mathrm{r}}x_{\mathrm{rd}}(t-1) + g_{\mathrm{e}}e(t-1), \quad (10)$$

where $x_{\mathrm{d}}(t-1) = (1-q^{-1})X_{\mathrm{a}}(t)$ and $x_{\mathrm{rd}}(t-1) = (1-q^{-1})x_{\mathrm{r}}(t)$, while the tracking criteria performance index can be written as

$$J = \sum_{t_0}^{\infty}\{(x_{\mathrm{d}}^{\mathrm{track}}(t))^{\mathrm{T}}Q^{\mathrm{track}}(x_{\mathrm{d}}^{\mathrm{track}}(t)) + v(t)^{\mathrm{T}}R^{\mathrm{track}}v(t)\} \quad (11)$$

where $x_{\mathrm{d}}^{\mathrm{track}}(t) = (1-q^{-1})x^{\mathrm{track}}(t+1)$, $v(t) = (1-q^{-1})u_{\mathrm{q}}(t+1)$, $Q^{\mathrm{track}} = C^{\mathrm{trackT}}C^{\mathrm{track}}$ and $R^{\mathrm{track}} > 0$ is a weighting factor for the incremental control input $v(t)$. Therefore, the optimal control having penalty on the error and the incremental error is given by

$$u_{\mathrm{q}}(t) = -K^{\mathrm{track}}x^{\mathrm{track}}(t)$$
$$u_{\mathrm{q}}(t) = -K_{\mathrm{a}}x_{\mathrm{a}}(t) - K_{\mathrm{r}}x_{\mathrm{r}}(t) - K_{\mathrm{e}}\textstyle\sum_{t_0}^{t-1}e(t) \quad (12)$$

where the optimal control gain matrix is given by

$$K^{\mathrm{track}} = [K_{\mathrm{a}(1\times6)} \quad K_{\mathrm{e}(1\times1)} \quad K_{\mathrm{r}(1\times2)}]$$
$$K^{\mathrm{track}} = (R^{\mathrm{track}} + B^{\mathrm{track}}PB^{\mathrm{track}})^{-1}B^{\mathrm{trackT}}PA^{\mathrm{track}}$$

and P is the solution of the following algebraic Riccati equation

$$A^{\mathrm{trackT}}PA^{\mathrm{track}} - P - A^{\mathrm{trackT}}PB^{\mathrm{track}}K^{\mathrm{track}} + Q^{\mathrm{track}} = 0 \quad (13)$$

A block diagram of the overall LQGR control system with integral action and desired temperature trajectory tracking is shown in Fig. 8. This controller guarantees the rejection of a constant disturbance and tracking of a desired temperature.

4. Results and discussion

The temperature control system described in Fig. 3 was built and assembled by the authors. This included a vacuum chamber (1 mTorr) and the temperature shield consisting of the copper ring and the sapphire plate. An analog amplifer to drive the thermo-electric heater/cooler and a low-noise bridge circuit for the thermistors were also custom designed and built. An optical readout system to produce the images from infrared source was also constructed. The control algorithm with a sampling time of 0.1 s was written in the 'C' programming language on a personal computer using a Data Translation DT322 16 bits analog-to-digital and digital-to-analog converters. The thermistor on the bottom of the heat sink chamber was used to measure the ambient temperature T_{a}. Its mean value was experimentally determined and it was used as the value of the deterministic disturbance temperature. The real time measurement of T_{a} was also used to linearize the dynamics of the thermo-electric heater/cooler using an algorithm described in [1]. Several typical experimental results are presented and described in this section. A comprehensive simulation study allowed us to select the initial values for the control parameters g_{e} in Eq. (9), R^{track} in Eq. (11). The dc gain and the time constant of the thermo-electic heater/cooler model were initially decided based on the details from its manufacture (Marlow MI1020T). Model identification and validation was based on matching transient responses. Appropriate model parameters were chosen and tunned so that the experimental and simulated results closely resembled each other, as shown in Figs. 9 and 10. Parameters of the thermo-electric heater/cooler model change easily

Table 1
Steady state simulated and experimental results of the LQGR control with penalty on the copper temperature T_{cu} with $g_{\mathrm{e}} = 1, R^{\mathrm{track}} = 0.1$.

Standard deviation	Unit	Simulation	Experiment
$\sigma_{T_{\mathrm{cu}}}^{\mathrm{measured}}$	mK	001.013	001.131
$\sigma_{\hat{T}_{\mathrm{cu}}}$	μK	046.43	061.52
$\sigma_{\hat{T}_{\mathrm{si}}}$	μK	069.23	073.77
$\sigma_{\hat{T}_{\mathrm{ch}}}$	μK	120.0	117.3

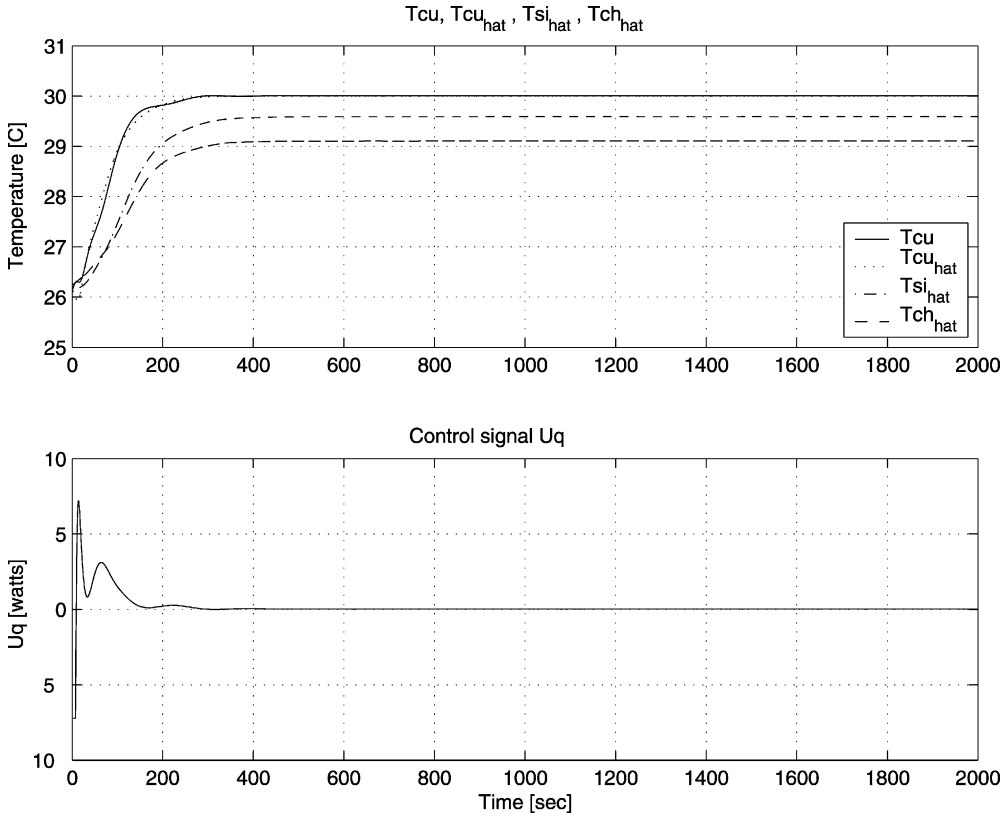

Fig. 9. Experimental results with $g_e = 1, R^{track} = 10$. $T_{cu}^{measured}$, $\hat{T}_{cu}$, $\hat{T}_{si}$ and $\hat{T}_{ch}$.

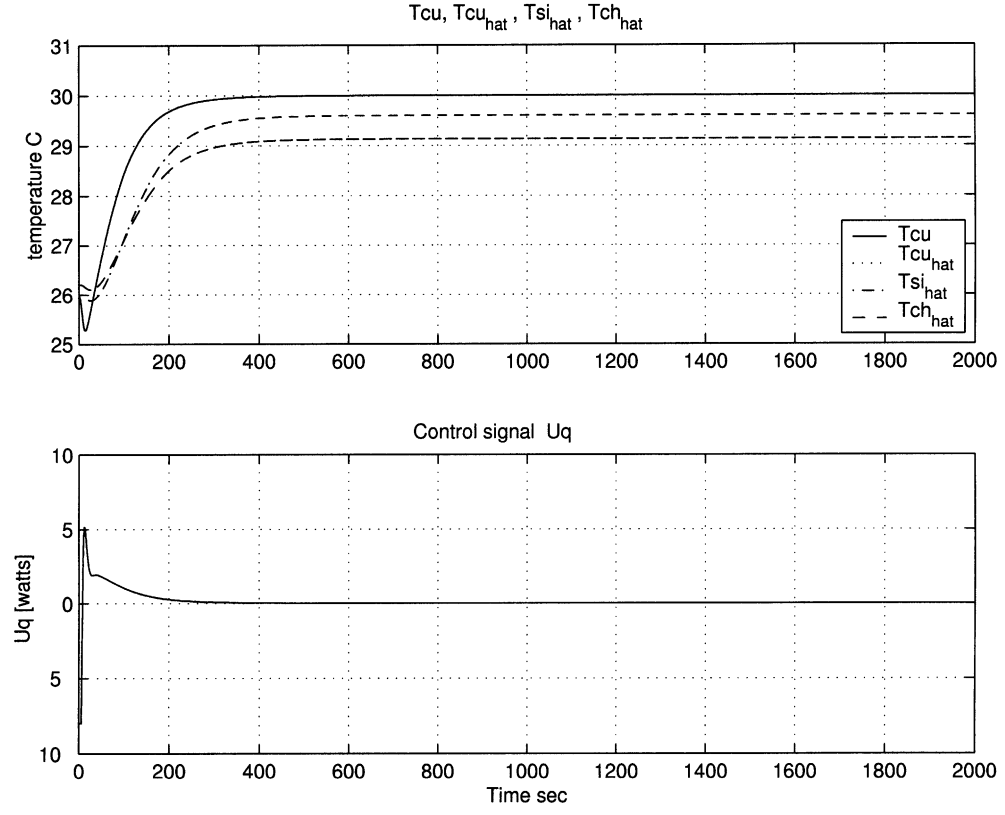

Fig. 10. Simulation results with $g_e = 1, R^{track} = 10$. $T_{cu}^{measured}$, $\hat{T}_{cu}$, $\hat{T}_{si}$ and $\hat{T}_{ch}$.

depending on operating conditions such as the chamber vacuum level, the quantity of thermal conductive paste that was used between the heater/cooler and the chamber floor and the operating temperature of the FPA. The heater/cooler model parameters were subsequently retuned to match the experimentally determined state estimation covariances to their corresponding simulation values, as shown in Table 1. However, transient responses in the experiment exhibited oscillatory modes, as the control penalty gain R^{track} was decreased, which were not observed in the simulation results. This is attributed to unmodeled dynamics between the copper ring and chip temperatures. Table 1 shows that simulation and the experimental results are in close agreement. With a copper ring temperature measurement noise that has a 1 mK standard deviation, the FPA T_{ch} temperature could be regulated to within a standard deviation of about 100 μK according to the estimated output value of $\hat{T}_{\text{ch}}$ from the designed Kalman filter as in Eq. (4). $\hat{T}_{\text{cu}}$, $\hat{T}_{\text{si}}$, and $\hat{T}_{\text{ch}}$ are not measured directly but are optimally estimated by the Kalman filter based on the measurement of T_{cu} and the stochastic model in Fig. 8. As shown in Table 1, the standard deviation of the FPA T_{ch} temperature is about twice as that of T_{cu}, due to the relatively large fluctuation in the sapphire plate temperature which had a standard deviation of 8.92 mK in the simulation results. Fig. 11 shows a close up of the steady state response for the measured copper temperature T_{cu}, the estimated copper temperature $\hat{T}_{\text{cu}}$, the estimated silicon temperature $\hat{T}_{\text{si}}$, as well as the estimated FPA temperature $\hat{T}_{\text{ch}}$. The Kalman filter output $\hat{T}_{\text{cu}}$ estimates well the measured temperature T_{cu}.

The noise equivalent temperature difference of an IR system is the smallest detectable temperature difference of the target source allowed by the system noise. In other words, the NETD is simply the system noise divided by the thermal sensitivity of the detector. To evaluate the sensitivity of the system, a black body source with temperature controlled to the resolution of ±0.05 K was used to provide a uniform calibrated IR flux onto FPA. The visible laser reflected from FPA was collected with a 12-bit digital CCD. By measuring the intensity change on the CCD pixels, we can obtain the system sensitivity as well as the overall system noise. The thermal sensitivity measured and calculated is about $\Delta T_{\text{FPA}}/\Delta T_{\text{target}} = 0.01$. The noise analysis indicates that there is long-term drift combined with short-term noise at frequencies between 1 and 10 Hz. The short-term noise represented by temperature fluctuation on FPA is measured to be around 2 mK, while the shot noise of the 12-bit digital CCD is about 1mK. The system noise is, therefore, reasonably close to the CCD shot noise. Details of the noise and sensitivity analysis are discussed in [3]. Theoretical noise calculations [10] are summarized in Table 2. The total system noise that is expressed as temperature fluctuation is the statistical average of all the noises in Table 2. Assuming that these individual noises ΔT_i are statistically uncorrelated, the total noise can be expressed as $\Delta T_{\text{total}} = \sqrt{\sum \Delta T_i^2}$, which is equal to 146 μK. The experimentally measured CCD noise and overall noise are larger than those of calculations in Table 2 because of dynamic range mismatches for FPA pixels' output onto the CCD, which is due to the non-uniform responses [7] of individual

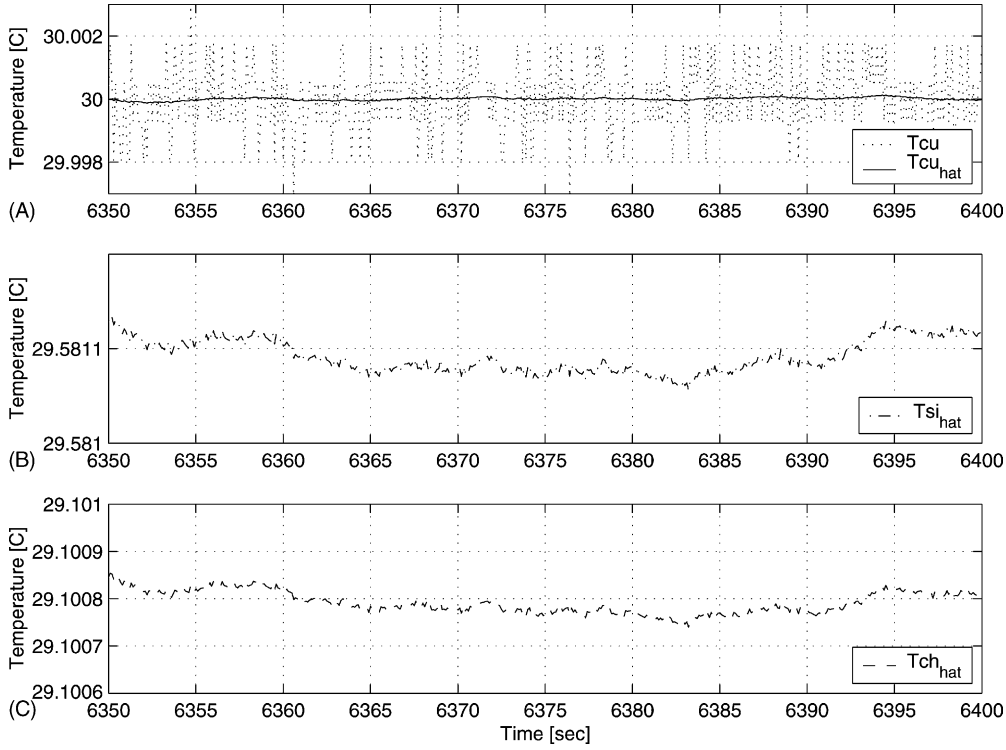

Fig. 11. Close up of the steady state experimental results with $g_{\text{e}} = 1, R^{\text{track}} = 0.1$. (A) $T_{\text{cu}}^{\text{measured}}$ and $\hat{T}_{\text{cu}}$ (B) $\hat{T}_{\text{si}}$ (C) $\hat{T}_{\text{ch}}$.

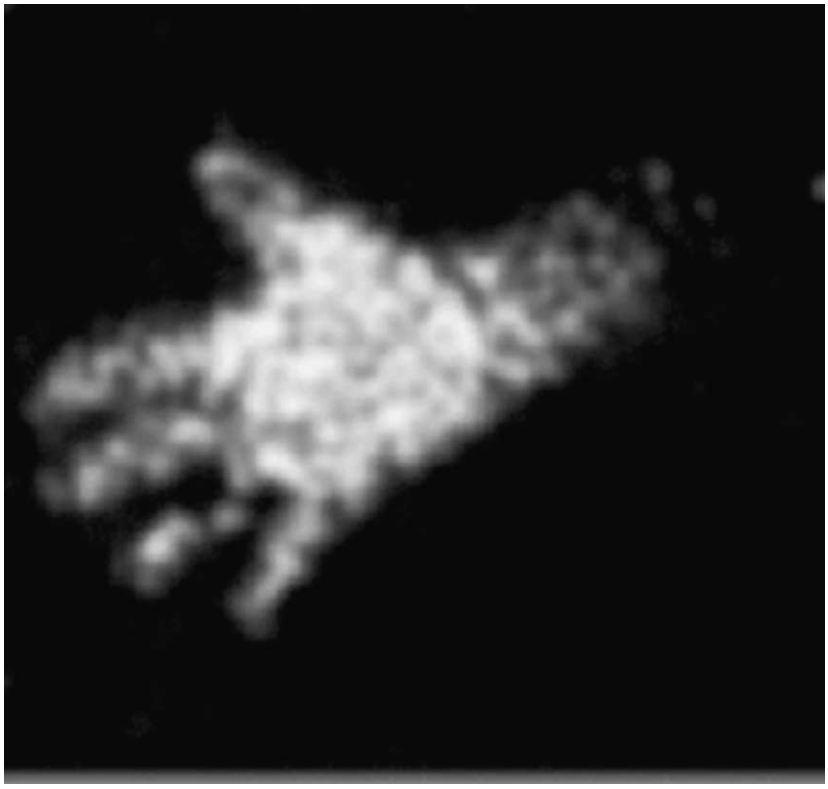

Fig. 12. Thermal image of a human hand using optomechanical uncooled infrared imaging camera at a distance of 2 m away with $f/1$ optics.

Table 2
Theoretical noise calculation analysis for MEMS optomechanical unclooled infrared imaging camera

ΔT_{th} (μK)	$\Delta T_{th,vib}$ (μK)	ΔT_{CCD} (μK)	ΔT_{laser} (μK)	ΔT_{FPA} (μK)	ΔT_{total} (μK)
51.7	1.26	65	19	120	146

ΔT_{th} is thermodynamic fluctuation noise, $\Delta T_{th,vib}$ is thermal vibration noise, ΔT_{CCD} is CCD noise, ΔT_{laser} is laser noise, ΔT_{FPA} is temperature stabilized FPA noise and ΔT_{total} is total noise.

FPA pixels. The empirical or simulation results of temperature stability of about 120 μK is negligible in the current setup. A measurement of the system sensitivity with a temperature controlled heat source shows that NETD of such uncooled IR system can reach 200 mK [7] at a frame rate of 10 Hz with $f/1$ optics. Fig. 12 shows a thermal image of a human hand taken by the designed IR camera system. More details on the determination of IR camera's NETD are presented in [7].

5. Conclusion

This paper presented the design and control of a thermal stabilizing system for an optomechanical uncooled infrared imaging camera. Experiments showed successful results for the prototype camera with the optical readout system. The thermal shield system provides a large amount of attenuation in open loop from disturbances in the ambient temperature T_a to FPA temperature T_{ch}. A carefully designed ambient temperature disturbance model was used to represent ambient temperature fluctuations, and this model was subsequently used in a model-based discrete linear time quadratic gaussian regulator (LQGR) control scheme. The LQGR controller was able to achieve an additional low frequency attenuation of more than 50 dB of disturbance rejection from the ambient temperature T_a to the FPA temperature T_{ch}. The disturbance attenuation was achieved without introducing any significant attenuation in the closed-loop sensitivity from the target temperature source T_t to T_{ch}, as shown in Fig. 5. The proposed control law includes a reference model to diminish overshoots and an integral action to achieve zero steady state error in closed loop, even in the presence of constant ambient temperature disturbances. Experimental results showed that the standard deviation of T_{ch} was around 100 μK as predicted by the analysis. Thus, the designed thermal isolation and regulation control system is well suited for the intended infrared imaging camera's purpose of accurately sensing the infrared source T_t. Noise analysis results for the present optomechanical infrared imaging system are summarized in Table 2. The NETD of current stage of the IR camera system can reach about 200 mK.

Acknowledgements

This project is supported by the DARPA IR program under grant N66001-00-C-8080.

References

[1] A.W. Sloman, P. Buggs, J. Molloy, D. Stewart, A Microcontroller-based driver to stabilize the temperature of an optical stage to within 1 mK in the range 4–38°C, using a Peltier heat pump and a thermistor sensor, Meas. Sci. Technol. 7 (1996) 1653–1664.
[2] Y. Zhao, J. Yamaguchi, J. Choi, S. Morales, R. Horowitz, A. Majundar, P. Norton, J. Kitching, H. Lin, M. Athavale, J. Varesi, Design and fabrication of an optomechanical uncooled infrared imaging system, in: Proceeding of the ASME IMECE Conference, 2001.
[3] Y. Zhao, M. Mao, R. Horowitz, A. Majundar, J. Varesi, P. Norton, J. Kitching, Optomechanical uncooled infrared imaging system: design, microfabrication and performance, JMEMS 11, (2) (2001) 136-146.
[4] T. Perazzo, M. Mao, O. Kwon, A. Majundar, J.B. Varesi, P. Norton, Infrared vision using micro-optomechanical camera, Appl. Phys. Lett. 74 (1999) 3567–3569.
[5] J. Choi, J. Yamaguchi, S. Morales, R. Horowitz, Y. Zhao, A. Majumdar, P. Norton, Design and control of a thermal stabilizing system for an optomechanical uncooled infrared imaging camera, in: Proceedings of the 15th IFAC World Congress, July 2002.
[6] R.R. Bitmead, M. Gevers, V. Wertz, Adaptive Optimal Control, Prentice-Hall, New York, 1990.
[7] Y. Zhao, J. Choi, S. Morales, J. Yamaguchi, R. Horowitz, A. Majumdar, P. Norton, J.E. Kitching, M.M. Athavale, Optomechanical uncooled infrared imaging system, in: Proceedings of SPIE Seattle, Seattle, WA, July 2002, p. 4820.
[8] B.D.O. Anderson, J.B. Moore, Optimal Control, Prentice-Hall, New York, 1989.
[9] F.P. Incropera, D.P. DeWitt, Fundamentals of Heat and Mass Transfer, fourth ed., Wiley, New York, 1996.
[10] H.W. Ott, Noise Reduction Techniques in Electronic Systems, second ed., Wiley, New York, 1988.
[11] Thermoelectric Cooling Systems Design Guide (MI1020T), Marlow Industries Inc., 2000.

Biographies

Jongeun Choi received the BS degree in Department of Mechanical Design and Production Engineering from Yonsei University, Seoul, South Korea, in 1998 and MS degree in Department of Mechanical Engineering from University of California, Berkeley, in 2002. He is currently pursuing PhD in Department of Mechanical Engineering from University of California, Berkeley. His research interests are control applications on MEMS sensor systems and self-organizing sensor array systems.

Yang Zhao received the BS and MS degrees in mechanical engineering from University of Science and Technology of China (USTC), Hefei, China, in 1994 and 1997, respectively. She is currently working towards the PhD degree in mechanical engineering at University of California, Berkeley. Her research interests include design and fabrication of MEMS and optical detection technique.

Roberto Horowitz received the BS degree with highest honors in mechanical engineering and the PhD degree from the University of California, Berkeley, in 1978 and 1983, respectively. He is currently a professor and the vice-chairman of graduate study in the Department of Mechanical Engineering, at University of California, Berkeley. He is teaching and conducting research in the areas of adaptive, learning, nonlinear and optimal control and mechatronics, with applications to disk file systems, robotics, microelectromechanical systems (MEMSs) and intelligent vehicle and highway systems.

Arunava Majumdar received the BTech degree in mechanical engineering from the Indian Institute of Technology, Bombay, India, in 1985 and the PhD degree in mechanical engineering from University of California, Berkeley, in 1989. He is currently a professor in the Department of Mechanical Engineering, University of California, Berkeley. Previously, he was with the Arizona State University, Temp, from 1989 to 1992 and the University of California, Santa Barbara (from 1992 to 1996) as a faculty member in mechanical engineering. His research interests in his group range from MEMS, micro/nanoscale thermophysics to nanobiomolecular engineering and nanoscale imaging. He is currently serving as an associate editor for the ASME Journal of Heat Transfer and the International Journal of Heat and Mass Transfer, and is co-editor-in-chief of Microscale Thermophysical Engineering. Dr. Majumdar is a recipient of the NSF Young Investigator Award, the ASME Melville Medal, and the ASME Best Paper Award from the Heat Transfer Division. He also serves as a member of the Council on Energy Engineering Research for the Department of Energy and the ASME Steering Committee on Nanotechnology.